# Volume index gratings in the intermediate and form-birefringence regimes

Cécile Joubert, Vincent Laude, Mane-Si Laure Lee, and Juliette Plouin

We present a study of volume index gratings operating in the form-birefringence regime and what we call the intermediate regime, defined as the regime between form birefringence and the onset of diffraction. The operating regime is characterized by the ratio between the measurement wavelength and the grating period: form birefringence regime below 10, diffraction around 3, and intermediate regime between 10 and 3. The behavior of the gratings in a given regime is studied by plotting the induced retardation as a function of the incidence angle. The shape of the curve fully characterizes the regime. We report on theoretical calculations of retardation by use of a rigorous theory and its experimental validation by measuring retardation of recorded gratings in photopolymers. © 2002 Optical Society of America

*OCIS codes:* 050.7330, 090.7330, 160.1190, 160.3710, 230.3720.

## 1. Introduction

The demand for liquid-crystal displays (LCD) panels is growing every day for various applications, such as for desktop computers, automotives, and avionics. LCDs offer high performance in terms of luminance, resolution, color, and gray-level capability, but the image degradation when the viewer moves away from the normal to the display is incompatible with the requirements of many applications of LCDs.

A solution to improve the viewing-angle characteristics of LCDs is the use of birefringent films positioned on each face of the LCD cell. To compensate for the LCD, the birefringent film, optimized by numerical simulation, must have precise values of retardation and orientation of optic axes.

It is well known that periodic dielectric layered media are effectively homogeneous and uniaxially birefringent when the wavelength of optical waves is much larger than the layer period.[1–3] This behavior is called form birefringence and can be characterized by effective medium theory (EMT) as a difference in permittivities for the two polarizations. Dielectric layered media were demonstrated to behave as synthetic materials with negative birefringence for twisted nematic (TN) LCDs viewing-angle compensation.[4] But large size manufacturing of such material at a reasonable cost is a delicate problem.

Another type of periodic structure that can be used in the form-birefringence regime are volume index gratings. Campbell *et al.*[5] described the behavior of sinusoidally modulated volume holograms in the form-birefringence regime by using EMT and found a direct relationship between the index modulation of the grating and the induced birefringence.

This theory is valid for grating periods that are less than one tenth of the optical wavelength. The achievement of form birefringence in volume holographic gratings has been experimentally verified by Kim *et al.*[6] and Yang *et al.*[7,8] with photopolymers as holographic media. All these gratings have been characterized by measuring the retardation at normal incidence.

From a practical point of view, well-known holographic media (mainly dichromated gelatine and photopolymer) are sensitive in the visible range and thus the available grating periods do not satisfy the effective-medium conditions. We call this situation, between form birefringence and diffraction, the intermediate regime. Joubert *et al.*[9] demonstrated the ability of volume index gratings, used in the intermediate regime, to compensate for TN-LCD, but a more

When this paper was written, the authors were with THALES Research and Technology FRANCE, Domaine de Corbeville, F-91404 ORSAY Cedex France. C. Joubert is now with NEMOPTIC, 1 rue Guynemer, F-78114 Magny les Hameaux, France. V. Laude is now with the Laboratoire de Physique et de Métrologie des Oscillateurs, CNRS UPR 3203, associé à l'Université de Franche-Comté, 32 avenue de l'Observatoire, F-25044 Besançon, France. J. Plouin is now with the Laboratoire de Physique et de Technologie des Plasmas, UMR 7648, Ecole Polytechnique F-91128 Palaiseau Cedex, France.

Received 1 March 2002; revised manuscript received 16 July 2002.

0003-6935/02/326751-12$15.00/0

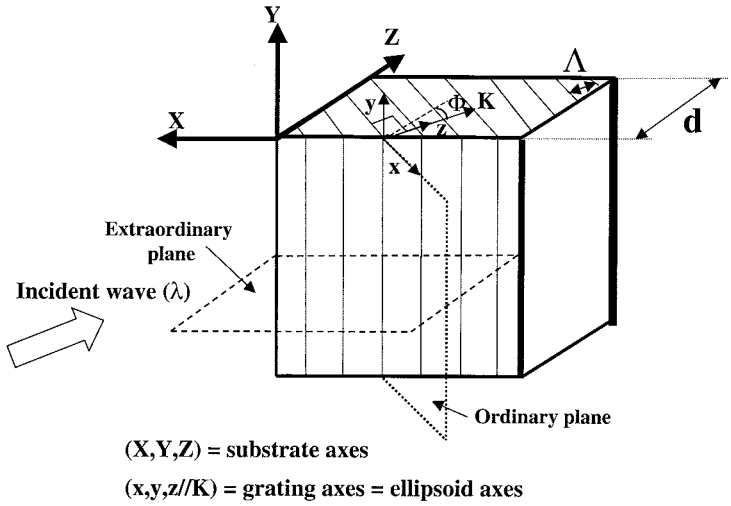


Fig. 1. Definition of substrate and grating related referential and grating parameters.

precise study of this regime still has to be done. Lalanne *et al.*[10] proposed a generalization of the EMT (the high-order EMT) providing accurate theoretical results of effective relative permittivity until illumination conditions close to the grating diffraction (grating period close to the optical wavelength).

An exact theory of planar and homogeneous volume index gratings, without any hypothesis on the illumination wavelength versus the grating period, was published by Moharam and Gaylord.[11] The present work investigates volume holographic gratings in the intermediate regime, defined as the regime between form birefringence and the onset of diffraction, both experimentally and theoretically. The gratings, recorded in a photopolymer from DuPont, are experimentally characterized by their retardation versus the angle of incidence, which is compared with the theoretical behavior of a uniaxial medium (the form-birefringence regime). The deviation from a uniaxial medium is the most important parameter for the use of these gratings for LCD compensation. The theoretical retardation in the intermediate regime is calculated by use of the Moharam and Gaylord theory. Different grating periods and layer orientations (unslanted and slanted gratings) as well as different illumination wavelengths have been subjected to our experiments and all the presented data are compared with the theoretical predictions.

## 2. Description of Different Regimes

### A. Definitions

Different theories describe the behavior of holographic gratings obtained by photoinduced index modulation. The modulation is assumed to be sinusoidal and the grating vector **K** is perpendicular to the index layers.

We define a referential (**X**, **Y**, **Z**) related to the grating substrate, with **Z** being the substrate normal (Fig. 1).

A volume index grating is defined by the following parameters (Fig. 1): **K** is the grating vector with $\mathbf{K} = 2 \cdot \pi/\Lambda \cdot \mathbf{z}$, **z** being the unitary vector parallel to $\mathbf{K} \cdot \Lambda$ is the grating period and $\phi$ is the index layer slant angle equal to the angle between **K** and the substrate normal **Z**, d is the grating thickness, $n_0$ the average index of the medium, and $n_1$ the amplitude of the sinusoidal index modulation. We define a referential related to the grating (**x**, **y** = **Y**, **z**$\|$**K**) (Fig. 1).

The illumination wave is characterized by the angle of incidence of the illumination (wavelength $\lambda$) in the medium. This angle of incidence is defined by the couple ($\alpha$, $\delta$) in the medium (Fig. 2). $\alpha$ is the angle between the index normal and the incident angle and $\delta$ is the tilt of the plane including the incident ray and **Z** with respect to the (**X**, **Z**) plane. The polarization is then defined by an angle $\Psi$ (Fig. 2).

As described in Ref. 5, we define two planes of interest, the ordinary and extraordinary planes (see Fig. 1). The extraordinary plane is the (**X**, **Z**) plane

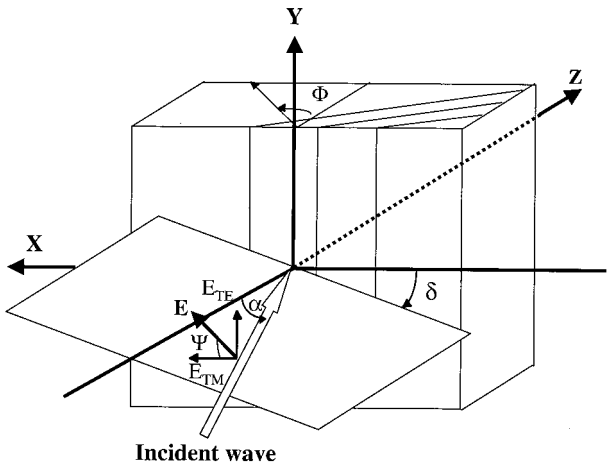


Fig. 2. Characterization of the illuminating wave.

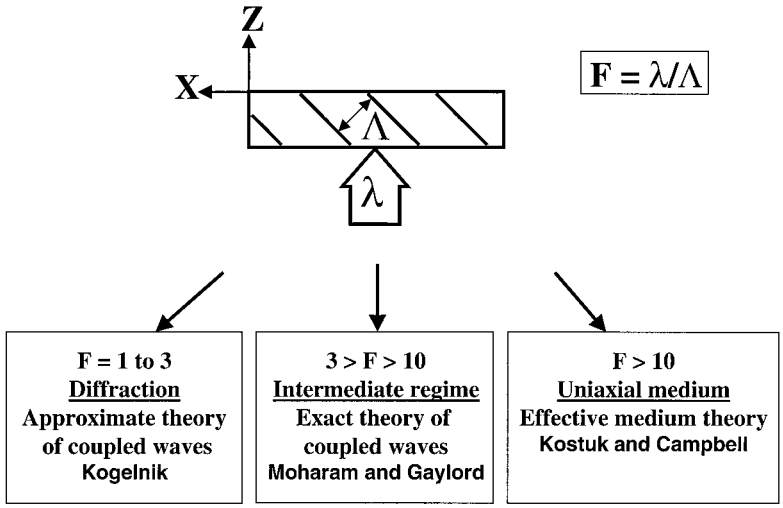


Fig. 3. Description of the three different regimes of a volume index grating as a function of $F = \lambda/\Lambda$.

and the ordinary plane is the ($\mathbf{x}$, $\mathbf{y} = \mathbf{Y}$) plane. The behavior of the grating will be studied with an illumination light incident in those two planes.

The factor F is $F = \lambda/\Lambda$, the wavelength to grating period ratio.

### B. Summary of Different Regimes

The regime where the grating operates is determined by the value of F (see Fig. 3): for F from 1 to 3, the illumination wavelength "sees" the grating, and we are in the diffraction regime described by the well-known coupled wave Kogelnik's[12] theory. For $F > 10$, the illumination wavelength does not see the grating but an average index: we are in the EMT,[5] and the index grating acts as a uniaxial medium with the optic axis parallel to $\mathbf{K}$. For $3 < F < 10$, we are in the intermediate regime that can only be described by an exact theory, such as that of Moharam and Gaylord.[11]

## 3. Theoretical Behavior of a Uniaxial Medium

A uniaxial medium is defined by the index ellipsoid as having three axes, with one of these axes being the optic axes. The ellipsoid axes corresponding to the grating of Figs. 1 and 2 in the form-birefringence regime is ($\mathbf{x}$, $\mathbf{y}$, $\mathbf{z}$) of Fig. 1. The behavior of a uniaxial medium can be characterized by plotting the retardation R (in nanometers) as a function of the incident light angle ($\alpha$, $\delta$).

The retardation is defined as

$$R(\alpha, \delta) = \Delta n(\alpha, \delta) \cdot e(\alpha, \delta) \tag{1}$$

(expressed in nanometers), where $\Delta n(\alpha, \delta)$ is the birefringence experienced by the illumination [$\Delta n(\alpha, \delta) = n(\alpha, \delta) - n_{or}$] and $e(\alpha, \delta)$ is the thickness of medium crossed by the illumination. We define the constant $R_0$ as $R_0 = (n_e - n_{or})d$, which is a retardation characterizing the medium. $R_0$ can be either positive ($n_e > n_{or}$, the positive uniaxial medium) or negative ($n_e < n_{or}$, the negative uniaxial medium).

### A. Extraordinary Plane

For an incident illumination in the extraordinary plane, containing the substrate normal $\mathbf{Z}$ and the optic axis $\mathbf{K}$, we have $\delta = 0$. The angle $\alpha$ (in the medium of index $n_0$) fully characterizes the incident angle. The perceived birefringence $\Delta n(\alpha)$ can be calculated, see Ref. 13, and is equal to

$$\Delta n(\alpha) = (n_e - n_{or}) \cdot \sin^2(\Phi - \alpha). \tag{2}$$

Thus the global retardation corresponding to an illumination with an incident angle $\alpha$ (in the medium) is

$$\begin{aligned} R(\alpha) &= \Delta n(\alpha) \cdot e(\alpha) \\ &= (n_e - n_{or}) \cdot \sin^2(\Phi - \alpha) \cdot \frac{d}{\cos \alpha}, \end{aligned} \tag{3}$$

with $e(\alpha) = (d/\cos \alpha)$.

So the quantity $R(\alpha)\cos \alpha$ is proportional to a square sine law

$$\begin{aligned} R(\alpha)\cos \alpha &= d \cdot (n_e - n_{or}) \cdot \sin^2(\Phi - \alpha) \\ &= R_0 \cdot \sin^2(\Phi - \alpha). \end{aligned} \tag{4}$$

- For $\alpha = \Phi$, $R(\alpha)\cos \alpha = 0$, the retardation is equal to zero, and the incident illumination is parallel to the optic axis.
- For $\alpha = \Phi \pm 90°$, $R(\alpha)\cos \alpha$ is maximum in absolute value, equal to $R_0$, and the incident illumination is perpendicular to the optic axis.

### B. Ordinary Plane

An incident wave in the ordinary plane is always perpendicular to the optic axis, so the perceived birefringence is always equal to the maximum medium birefringence ($n_e - n_{or}$). We characterize the incidence in this plane by the angle $\beta$, which is equal to the angle between the incident ray and $\mathbf{x}$ (Fig. 4). Each value of $\beta$ corresponds to a different value of ($\alpha$,

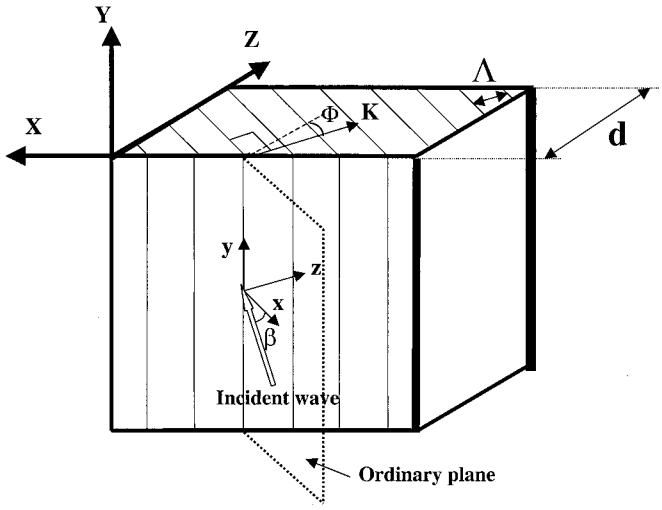


Fig. 4. Description of the ordinary plane of incidence.

δ) defined above. The relations between β and (α, δ) are

$$\cos \alpha = \sin \Phi \cos \beta, \tag{5}$$

$$\tan \delta = -\tan \beta / \cos \Phi. \tag{6}$$

Thus

$$\Delta n(\beta) = (n_e - n_{or}) \tag{7}$$

whatever β equals in the ordinary plane.

The thickness of the medium crossed by the illumination in this plane is

$$e(\beta) = \frac{\mathrm{d}}{\sin \Phi \cdot \cos \beta}. \tag{8}$$

Then

$$\mathrm{R}(\beta)\cos \beta = (n_e - n_{or}) \frac{\mathrm{d}}{\sin \Phi} = \frac{\mathrm{R}_0}{\sin \Phi} \tag{9}$$

is a constant whatever β equals in the ordinary plane, and

$$\mathrm{R}(\beta)\cos \alpha = \mathrm{R}_0. \tag{10}$$

Thus a uniaxial medium can be characterized by the measurement of the retardation $\mathrm{R}(\alpha)\cos \alpha$ versus the angle of incidence (in the medium) in specific planes

- Extraordinary plane: sine square law for $\mathrm{R}(\alpha)\cos \alpha$;
- Ordinary plane: constant for $\mathrm{R}(\beta)\cos \beta$ or $\mathrm{R}(\beta)\cos \alpha$.

#### 4. Effective Medium Theory

The EMT, valid when $\mathrm{F} > 10$, is described by Campbell *et al.* in Ref. 5, 6. The principal result of this theory is that the sinusoidally modulated volume grating is equivalent to a uniaxial medium with the optic axis parallel to the grating vector **K** and a birefringence $(n_e - n_{or})$ directly proportional to the index modulation $n_1$ of the grating[6]

$$n_e - n_{or} = -\frac{{n_1}^2}{n_0}. \tag{11}$$

A volume index grating is thus equivalent to a negative uniaxial medium, $\mathrm{R}_0 < 0$. This is illustrated in Fig. 5.

Typical values for photopolymers from DuPont are $n_0 = 1.51$, $n_1 = 0.05$, and $d = 25$ μm; thus the

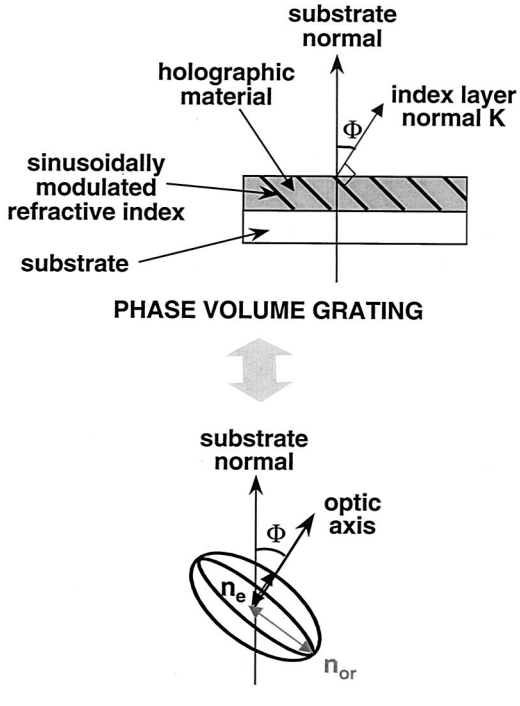


Fig. 5. Phase volume grating behavior when in accordance with the effective medium theory.

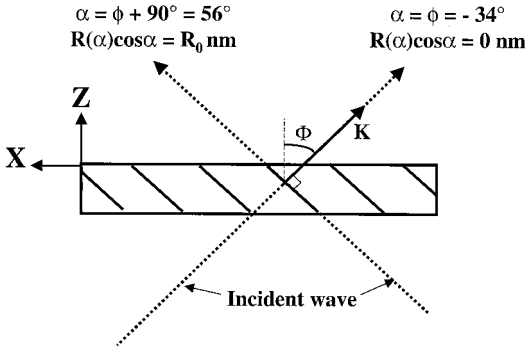


Fig. 6. Induced retardation R of a slanted volume grating in accordance with the effective medium theory for two specific angles of incidence in the medium in the extraordinary plane: $\alpha = \Phi$ and $\alpha = \Phi \pm 90°$.

birefringence is $(n_e - n_{or}) = 1.8 \times 10^{-3}$ and the retardation $R_0$ is $R_0 = -40$ nm.

Let us take an example with $\Phi = -34°$, which will be of interest for experimental results (Fig. 6).

The theoretical behavior of this grating, described with the evolution of $R(\alpha)\cos\alpha$ versus $\alpha$ as explained in Section 3, is drawn in Fig. 7(a) for the extraordinary plane; the evolution of $R(\beta)\cos\beta$ versus $\beta$ is shown in Fig. 7(b) for the ordinary plane.

We study the grating in the intermediate regime next.

## 5. Intermediate Regime

### A. Frontier between Intermediate and Diffraction Regimes

The intermediate regime is limited by the appearance of diffraction. The diffraction is determined by the Bragg condition (expressed in the extraordinary plane)

$$\frac{2n_0\Lambda}{\lambda}\cos(\Phi - \alpha) = 1, \tag{12}$$

that is to say,

$$\frac{2n_0}{F}\cos(\Phi - \alpha) = 1. \tag{13}$$

The appearance of diffraction is thus determined by the value of F, and the values of angles $\alpha$ and $\Phi$.

When $2n_0/F\cos(\Phi - \alpha) < 1$, that is to say $F > 2n_0\cos(\Phi - \alpha)$, we are in the intermediate regime. In particular, if $F > 2n_0$, we are always in the intermediate regime. For photopolymers $n_0 = 1.51$, thus when $F > 3$, we are in the intermediate regime whatever the values of $\alpha$ and $\Phi$.

### B. Principle of the Calculation

The retardation can be computed by use of the rigorous diffraction theory of planar dielectric gratings of Moharam and Gaylord.[11] No approximation is made regarding the thickness or the index modulation depth, and Maxwell's equations are solved exactly. An arbitrary number of diffraction orders, either propagating or evanescent, are taken into account.

The main output of the computation is the phase and amplitude of every diffraction order along the **X**, **Y** and **Z** axes (Fig. 2) for an incident plane wave specified by angles $\alpha$, $\delta$, and $\psi$. In the case we consider here, no propagating diffraction orders exist except for the zeroth order. Seven diffraction orders $-3 \ldots 3$ were taken into account in the computations, and it was verified that including more orders did not improve the results.

The geometry used for the computation is shown in Fig. 2. Following Ref. 11, all vector quantities are expressed relative to the (**X**, **Y**, **Z**) referential linked to the substrate.

Computing the retardation $R(\alpha, \delta)$ mainly involves evaluating the TM and TE phases of the output zeroth order. The retardation is directly related to the

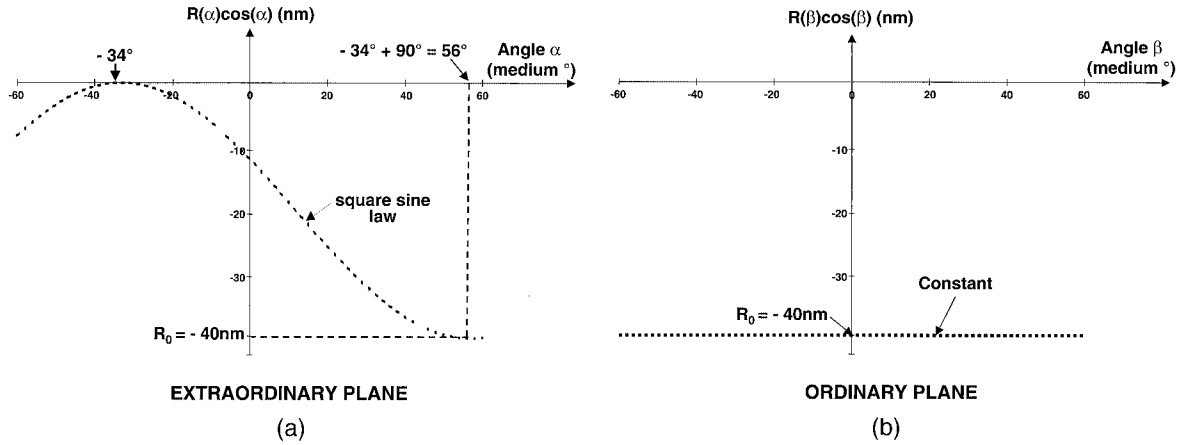


Fig. 7. Theoretical behavior of R ($\alpha$ or $\beta$, respectively) cos $\alpha$ (or cos $\beta$, resp.) as a function of $\alpha$ or resp. $\beta$, respectively for a uniaxial medium: (a) extraordinary plane, square sine law; (b) ordinary plane, constant.

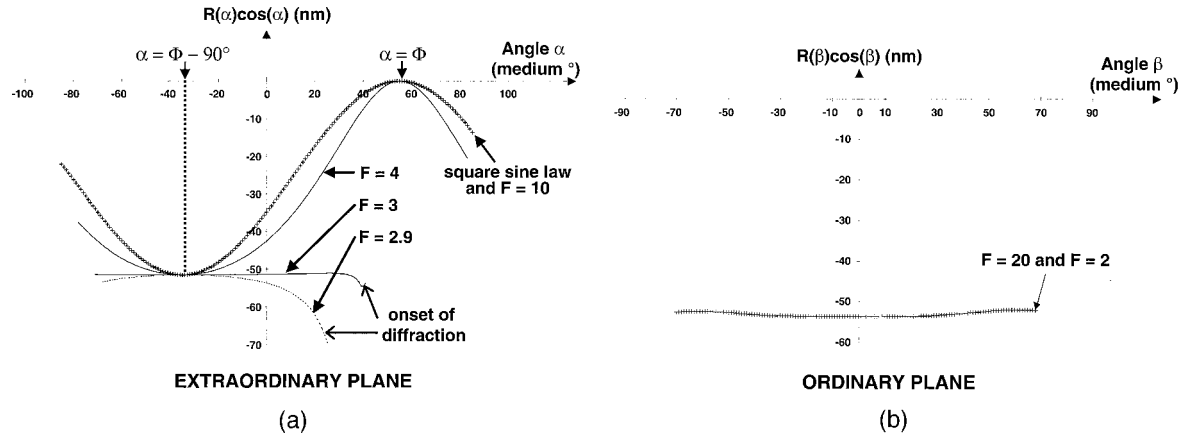


Fig. 8. Theoretical behavior of retardation versus α of a grating with $\Phi = 56°$ and $R_0 = -52$ nm, for different values of F between 10 and 2.9. (a) extraordinary plane, progressively away from the square sine law when F decreases; (b) ordinary plane, constant whatever the F value.

TM- and TE-induced phases by the well-known relation:

$$R(\alpha, \delta) = \frac{\lambda}{2\pi}[\varphi_{TM}(\alpha, \delta) - \varphi_{TE}(\alpha, \delta)]. \qquad (14)$$

The extraordinary plane coincides with the (**X**, **Z**) plane, and the incidence in this plane is obtained by setting $\delta = 0$ and varying α as explained in Section 3. Assuming the input polarization to be $\Psi = \pi/4$, the TM phase is obtained along the **X** axis, while the TE phase is obtained along the **Y** axis. For every incidence angle, the retardation is obtained by using a single computation instead of two.

The ordinary plane has a rather arbitrary orientation with respect to the substrate and the computation of the retardation is a little more intricate. Incidence in this plane is measured by angle β (see Fig. 3). From β, angles α and δ are obtained by using Eqs. (5) and (6), respectively. TE polarization is then obtained with

$$\tan \Psi = \tan \Phi \cdot \sin \alpha \cdot \sin \delta, \qquad (15)$$

and the TE phase is then found along the $-\mathbf{X}$ axis.

TM polarization is obtained by a $-\pi/2$ rotation from the TE angle, and the TM phase is then found along the **Y** axis. Thus for every incidence angle in the ordinary plane, the retardation is obtained by using two distinct computations.

### C. Simulation Example

By using the method described above, the behavior of the grating in the ordinary and extraordinary plane has been simulated for different values of F related to the values reachable in the experiments.

Figures 8(a) and 8(b) show the retardation versus α of a grating with $\Phi = 56°$ and $R_0 = -52$ nm, for different values of F between 2.9 and 10.

On Figure 8(a) we see that the shape of the curve moves progressively away from the sine square law ($F > 10$), first keeping the same monotony until $F = 4$, then becoming flat, and at the end diverging when approaching the diffraction regime, $F \cong 3$. For $F = 3$ the corresponding $\alpha_{diff}$ is $\alpha_{diff} = 49.4°$ and for $F = 2.9$, $\alpha_{diff} = 39.8°$.

The maximum retardation value (in absolute value) $R_0$ obtained for $\alpha = \Phi \pm 90°$ stays identical whatever the regime. Thus the experimental measurement of $R_0$ will give in any case a precise determination of $n_1$, by using formula (9).

In Fig. 8(b) we observe that in the ordinary plane, the retardation acts similarly; in the form birefringence and the intermediate regimes: The quantity $R(\beta)\cos \alpha$ is equal to $R_0$ whatever the value of β and F.

It can be seen that the shape of the retardation versus the incident angle in the extraordinary plane is directly related to the ratio of $F = \lambda/\Lambda$.

### D. Sensitivity to Grating Slant

We simulated a typical volume holographic grating recorded in photopolymers ($n_1 = 0.056$ and $d = 24.8$ μm) with three different values of the slant angle Φ: 0°, 45°, and 90°. We plotted in Fig. 9(a) [respectively 9(b) and 9(c)] the retardation versus α for $\Phi = 0°$ (respectively $\Phi = 45°$ and $\Phi = 90°$) in the extraordinary plane, for four values of F (10, 4.63, 3.77, and 3.35) corresponding to experimentally accessible values of the illumination wavelength λ and grating period Λ (see the experimental results below).

It can be seen that the shape of the curves and their evolution with F are identical for the three values of Φ. The slant angle is not a significant parameter for the behavior of the grating. When F decreases from 10 to 3.35, we note that the shape of the curve continuously moves away from the sine square law, keeping the same monotony.

## 6. Experimental Assessment

We performed an experimental validation of the theoretical behavior described above. Index gratings were recorded. The retardation versus the incidence angle was measured and compared with the theoretical predictions.

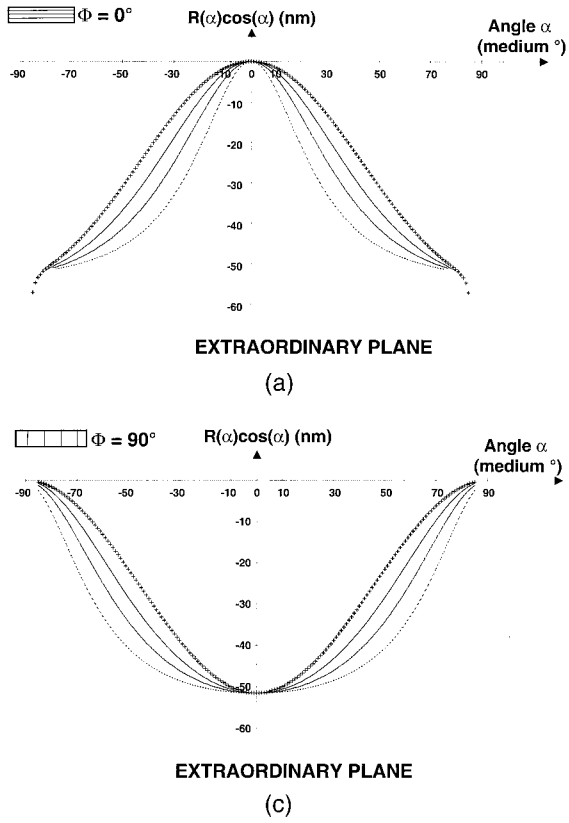


Fig. 9. Simulated typical volume holographic grating recorded in photopolymers ($n_1 = 0.056$ and $d = 24.8$ μm). Evolution of retardation versus incidence in the extraordinary plane for four values of F: (crosses) F = 10 (square sine law), (solid curve) F = 4.63, (dashed curve) F = 3.77, (dotted curve) F = 3.35. (a), Slant angle Φ = 0°; (b), slant angle Φ = 45°; (c), slant angle Φ = 90°.

### A. Recording Geometry

First, index modulation gratings were recorded in three different geometries (see Fig. 10) to obtain different grating periods Λ and slant angles Φ. The holographic recording is classical: the photosensitive medium is positioned in the interference field of two coherent plane waves of wavelength $\lambda_0$.

Let us call $\theta_1$ and $\theta_2$ the angles of incidence of the interfering beams with respect to the recording medium substrate normal. The theoretical grating parameters $\Lambda_{th}$ and $\Phi_{th}$ can be calculated as a function of $\theta_1$, $\theta_2$, $\lambda_0$, and $n_0$ (average index of the material) by the following formulas

$$\Lambda_{th} = \frac{\lambda_0}{2n_0 \sin(|\theta_1 - \theta_2|/2)}, \tag{16}$$

$$\Phi_{th} = \frac{\theta_1 + \theta_2}{2} + 90° \cdot \text{sign}(\theta_1 - \theta_2). \tag{17}$$

The different values of $\Lambda_{th}$ and $\Phi_{th}$ corresponding to the three recording geometries are calculated in Table 1 for $\lambda_0 = 413$ nm and $n_0 = 1.51$.

Let us refer to H34, H45, and H90 as the three recorded index gratings with the slant angle Φ equal respectively to −34°, −45°, and −90°.

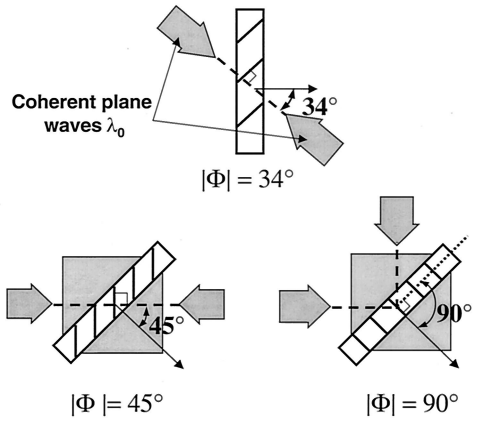


Fig. 10. Classical recording of index modulation gratings in three different geometries.

### B. Recording with DuPont Photopolymers

Index modulation gratings were recorded by using photopolymers from DuPont as the recording material.[14] The photopolymer solution is spin coated on a glass substrate. The recording process consists of

**Table 1. Grating Parameters (Λ Period, Φ Slant Angle)**[a]

| $\theta_1$ | $\theta_2$ | $\Lambda_{th}$ | $\Phi_{th}$ |
|---|---|---|---|
| −34° | 146° | 136.8 nm | −34° |
| −45° | 135° | 136.8 nm | −45° |
| −45° | 45° | 193.4 nm | −90° |

[a]As a function of the recording beams incidence angles ($\theta_1$, $\theta_2$).

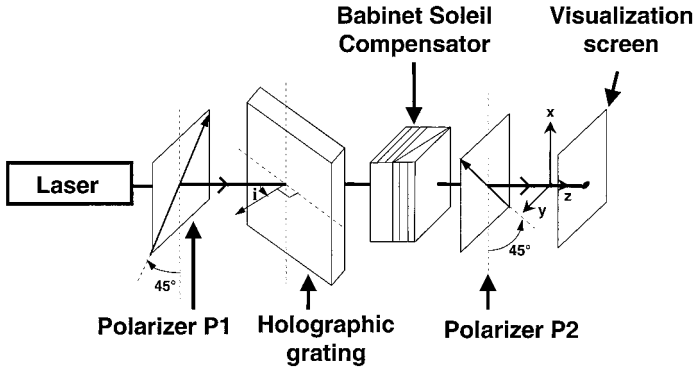


Fig. 11. Experimental setup for the measurement of the retardation introduced by the index modulation grating at different incidences $i$ with a Babinet Soleil compensator.

three steps: (1) recording of the grating. Typical required energy value is 20 to 50 mJ/cm$^2$ for the visible wavelength, 413 nm included. (2) UV irradiation and (3) curing during 2 h at 120 °C.

The complete process slightly modifies the grating parameters $\Lambda$ and $\Phi$. A shrinkage or swelling of a few percent of $\Lambda$ is usually observed. The slant angle remains mainly constant, therefore we will consider it unchanged by post processing.

### C. Experimental Determination of Grating Parameters

The thickness of the grating layer $d$ is directly measured. The index modulation $n_1$ is determined by measuring the maximum retardation $R_0$ (see below) in the extraordinary plane at $\alpha = \Phi \pm 90°$ and applying relations (5) and (11) with $n_0 = 1.51$. The value of $R_0$, and thus that of $n_1$, depends on the characterization wavelength $\lambda_c$.

### D. Experimental Measurements of Retardation versus Angle of Incidence

The retardation introduced by the index modulation grating is measured by a Babinet Soleil compensator.[15] The experimental setup is shown in Fig. 11. The angle of incidence $i$ of light coming from the laser is either $\alpha$ (extraordinary plane) or $\beta$ (ordinary plane)

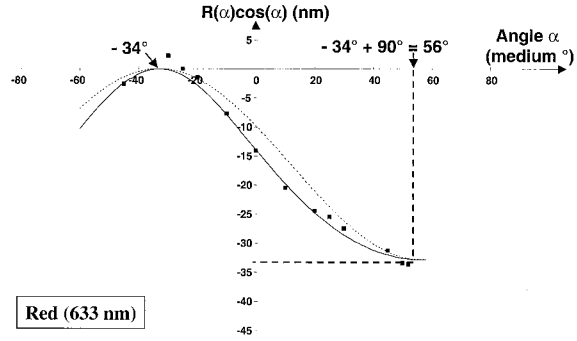


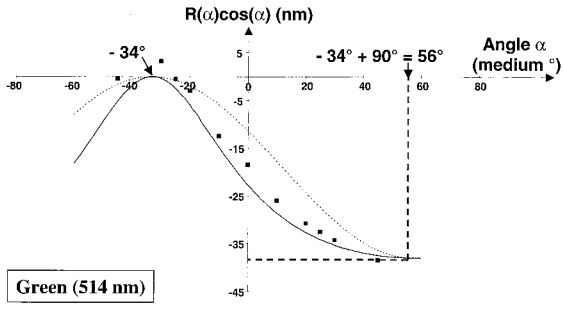


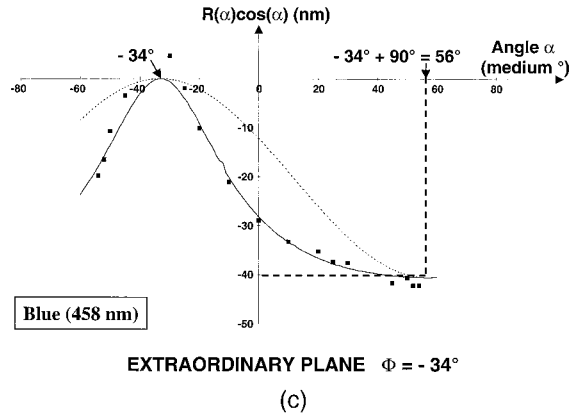


Fig. 12. Comparison between experimental and theoretical curves of retardation versus incidence in the extraordinary plane for recorded index grating H34 ($\Phi = -34°$): (dashed curve), square sine law, (solid curve) rigorous theory of coupled waves, (filled squares) experimental data. (a) Characterization wavelength $\lambda_c = 628.8$ nm (red), F = 4.69; (b) characterization wavelength $\lambda_c = 514$ nm (green), F = 3.57; (c) characterization wavelength $\lambda_c = 458$ nm (blue), F = 3.18.

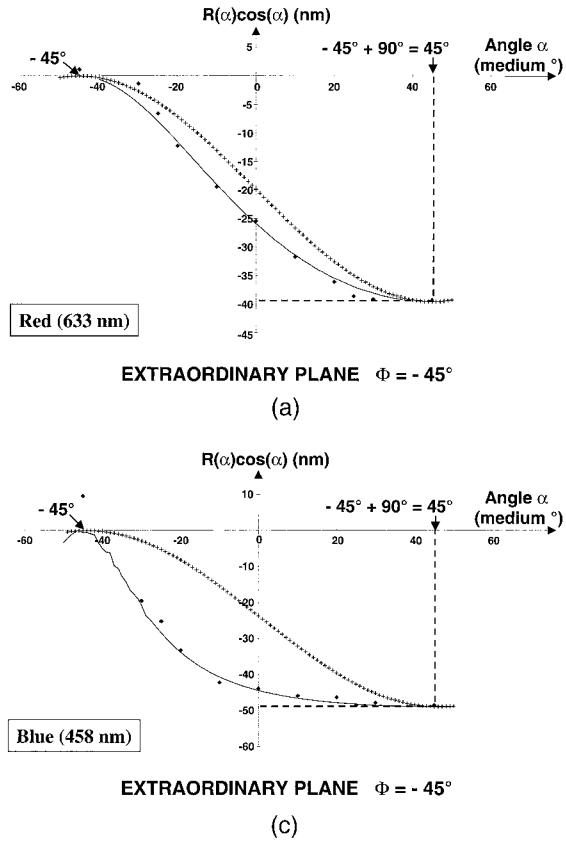


Fig. 13. Comparison between experimental and theoretical curves of retardation versus incidence in the extraordinary plane for recorded index grating H45 ($\Phi = -45°$): symbols same as Fig. 12.

depending on the orientation of the grating. Thus the retardation versus the incidence curve can be measured either in the ordinary or extraordinary plane. The Babinet compensator is aimed at analyzing an elliptically polarized wave. When one of the index ellipsoid axes of the component to be characterized is parallel to one of the Babinet-compensator axes ($x$ or $y$, see Fig. 11), the compensator measures the retardation between the extraordinary and ordinary waves passing through the component.[15] First, the incident beam is linearly polarized by the polarizer $P_1$. The zero of the Babinet is achieved when the compensator does not modify the polarization, i.e., when an extinction of the output beam is obtained, with $P_2$ perpendicular to $P_1$. Then, the holographic component is inserted between $P_1$ and the compensator. The beam arriving on the compensator is thus elliptically polarized. By translating the wedges of the Babinet, the extinction can be recovered. Finally, as the translation distance is directly proportional to the retardation between the extraordinary and ordinary waves passing through the component, by measuring the translation distance it is possible to obtain the retardation.

Two lasers have been used for the measurements to obtain wavelength characterizations covering the entire visible spectrum: a He–Ne laser for the red (632.8 nm) and an Argon laser for the green (514 nm) and the blue (458 nm).

Figures 12(a), 12(b), 12(c), 13(a), 13(b), 13(c), 14(a), 14(b), and 14(c) show the measured retardation $R(\alpha)\cos\alpha$ versus the angle of incidence in the medium $\alpha$ ($n_0 = 1.51$) in the extraordinary plane. Figures 12, 13, and 14 correspond respectively to the three recorded gratings H34 with slant angle $\Phi = -34°$, H45 with $\Phi = -45°$, and H90 with $\Phi = -90°$, and subfigures (a), (b), (c), respectively to the red, green, and blue characterization wavelength. Figure 15 shows the behavior of the H90 grating in the ordinary plane.

### E. Calculation of Theoretical Curves

Two simulated curves of retardation versus incidence are superposed to the experimental measurements in Figures 12, 13, and 14. One corresponds to a uniaxial behavior and is a sinusoid as described by relation (6), while the other is the calculated behavior in the intermediate regime by use of the Moharam and Gaylord rigorous diffraction theory. The different parameters needed for the computation are the following:

For each recorded grating, well-known parameters are slant angle $\Phi$, characterization wavelength $\lambda_c$, and average refraction index $n_0$ equal to 1.51. Measured parameters are thickness $d$, and index modulation $n_1$ (see above) as a function of $\lambda_c$. The only adjusted parameter of the simulation is the grating period $\Lambda$ in a range not exceeding $\pm 5\%$ of the theoretical value $\Lambda_{th}$. This adjustment is justified by the fact that the grating period is slightly modified by the post processing. The chosen value $\Lambda_{opt}$ is the value giving the best fit between experimental and theoretical curves. For each grating the same $\Lambda_{opt}$ is of course used for the three simulations with red, green,

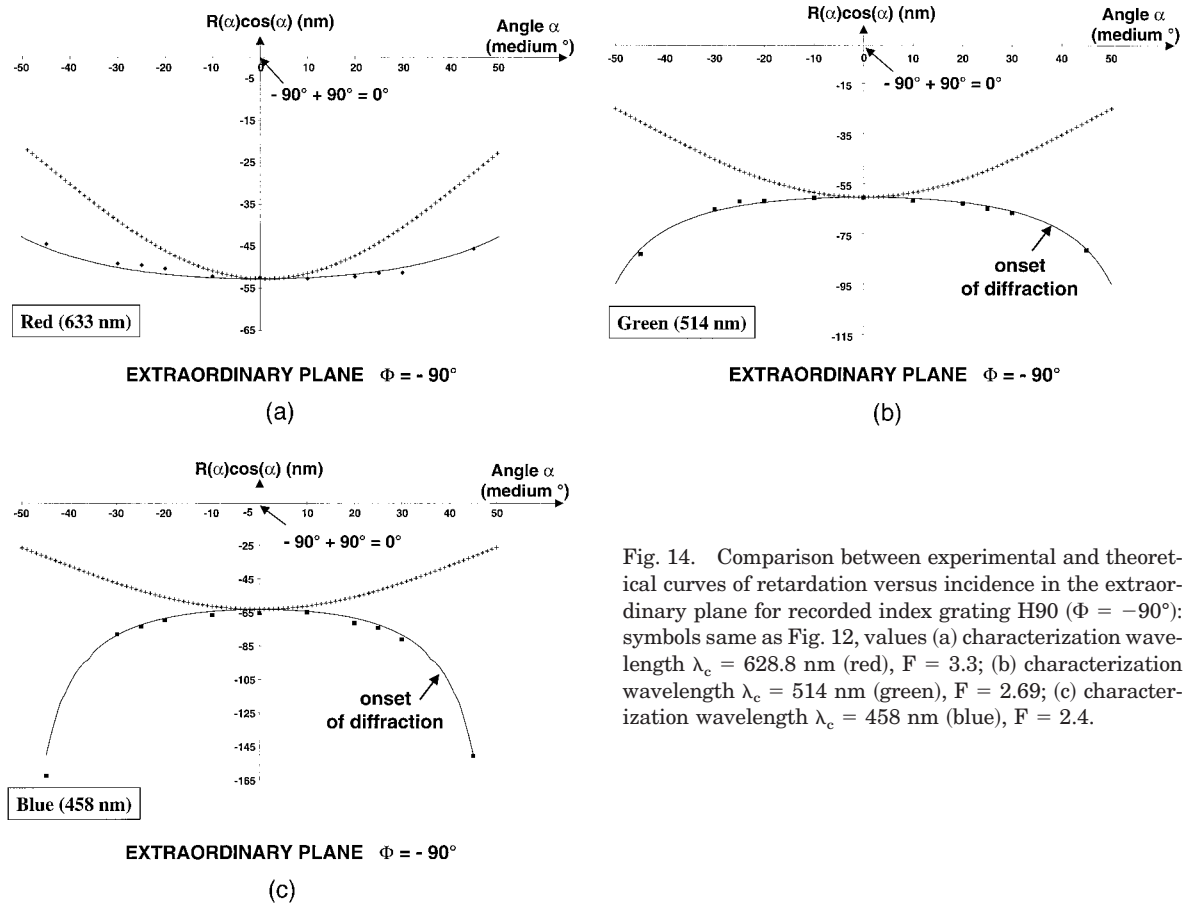


Fig. 14. Comparison between experimental and theoretical curves of retardation versus incidence in the extraordinary plane for recorded index grating H90 ($\Phi = -90°$): symbols same as Fig. 12, values (a) characterization wavelength $\lambda_c = 628.8$ nm (red), $F = 3.3$; (b) characterization wavelength $\lambda_c = 514$ nm (green), $F = 2.69$; (c) characterization wavelength $\lambda_c = 458$ nm (blue), $F = 2.4$.

and blue characterization wavelengths. For the calculations the parameter $F = \lambda_c/\Lambda_{opt}$ that characterizes the grating behavior in the intermediate regime. Table 2 summarizes the values of the parameters used for each simulation.

### F. Comparison between Experimental and Theoretical Curves

It can be seen in Figs. 12 to 15 that a good agreement is obtained between the experimental measurements

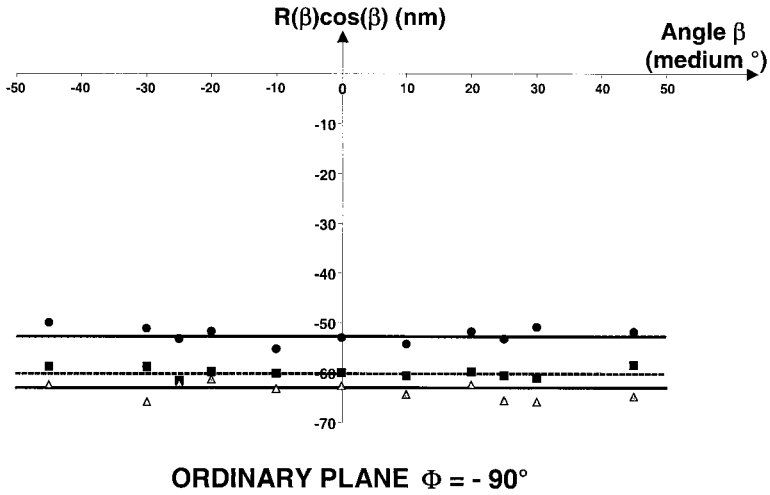


Fig. 15. Comparison between experimental and theoretical curves of retardation versus incidence in the ordinary plane for the recorded index grating H90 ($\Phi = -90°$) for the three characterization wavelength $\lambda_c$. $\lambda_c = 628.8$ nm (red), $F = 3.3$ and $R_0 = -53$ nm, solid line, rigorous theory of coupled waves, filled circles, experimental data; $\lambda_c = 514$ nm (green), $F = 2.69$ and $R_0 = -61$ nm, dashed line, rigorous theory of coupled waves, solid squares, experimental data; $\lambda_c = 458$ nm (blue), $F = 2.4$ and $R_0 = -63$ nm, gray line, rigorous theory of coupled waves, open triangles, experimental data.

Table 2. Parameters of Recorded Gratings Used in the Calculation

| Gratings | Slant $\Phi$ (°) | Thickness d ($\mu$m) | Period $\Lambda_{th}$ (nm) | Period $\Lambda_{opt}$ (nm) | Characteristics $\lambda_c$ (nm) 632.8 | Characteristics $\lambda_c$ (nm) 514 | Characteristics $\lambda_c$ (nm) 458 |
|---|---|---|---|---|---|---|---|
| H34 | −34 | 30.2 | 136.8 | 144 | $R_0 = -33$ nm | $R_0 = -38$ nm | $R_0 = -40$ nm |
| | | | | +5% $\Lambda_{th}$ | $n_1 = 0.0405$ | $n_1 = 0.0435$ | $n_1 = 0.045$ |
| | | | | | F = 4.39 | F = 3.57 | F = 3.18 |
| H45 | −45 | 29.5 | 136.8 | 144 | $R_0 = -40$ nm | $R_0 = -44$ nm | $R_0 = -49$ nm |
| | | | | +5% $\Lambda_{th}$ | $n_1 = 0.045$ | $n_1 = 0.0475$ | $n_1 = 0.05$ |
| | | | | | F = 4.39 | F = 3.57 | F = 3.18 |
| H90 | −90 | 24.8 | 193.4 | 191 | $R_0 = -53$ nm | $R_0 = -61$ nm | $R_0 = -63$ nm |
| | | | | −1% $\Lambda_{th}$ | $n_1 = 0.057$ | $n_1 = 0.061$ | $n_1 = 0.062$ |
| | | | | | F = 3.3 | F = 2.69 | F = 2.4 |

and the calculations performed with the exact diffraction theory in the intermediate regime, thus validating the accuracy of the behavior modeling of index gratings presented in this paper.

In the extraordinary plane we observe from Table 2 that the situation where H34 and H45 are characterized with red, green, and blue wavelengths, and H90 with red, corresponds to a factor F between 3 and 10 (intermediate regime, see Subsection 2.B). The more F is close to 3, the more the curves move from the sine square law corresponding to the form-birefringence regime, but keeping the same monotony. When F is smaller than 3, the characterization wavelength starts to "see" the grating, and the curves shape (H90 with green and blue) becomes divergent. This behavior is predicted by the calculations, and the experimental data are in a very good accordance with the predictions. Positive values of experimental retardation measured at the incidence angles around $\Phi$ are due to parasitic gratings recorded at the same time as the main grating that introduce small form birefringence.

In the ordinary plane we can see that the curves shapes remain constant whatever the value of F, as predicted by the modeling.

The value of $R_0$, measured at an angle of incidence of $\Phi \pm 90°$, is constant whatever the regime and is directly related to the index modulation $n_1$ by Eqs. (4) and (9). $R_0$ measurement is then a precise determination of the index grating modulation. The value of $n_1$ slightly depends on the characterization wavelength $\lambda_c$, which decreases when $\lambda_c$ increases.

## 7. Conclusion

We have presented in this work a detailed study of the behavior of index modulation gratings in the intermediate regime, i.e., between form birefringence and diffraction. The values of the retardation R versus the angle of incidence in specific planes, called extraordinary and ordinary planes, fully characterize the grating properties, mainly depending of the ratio F between characterization wavelength and grating period: a quasi-sinusoidal shape of R is obtained for $F > 4$ and corresponds to a situation close to form birefringence (the effective medium theory). For a value of F between 4 and 3, R continuously moves from a sinusoid (the intermediate regime), and for F around 3 (close to diffraction) R becomes divergent. Precise determination of the values of R versus the angle of incidence has been obtained by simulation by use of a rigorous diffraction theory. Experimental validation of the model has been demonstrated by measuring R versus the angle of incidence of index modulation gratings recorded with DuPont photopolymers. The experimental results have been compared to rigorous calculations, and a good accordance has been obtained. For the first time to our knowledge a complete comparison between theory and experiment has been performed for index modulation gratings operating in the intermediate regime by studying the curve shape of retardation versus the angle of incidence.

To use holographic gratings as uniaxial-media compensators for liquid-crystal displays it is necessary that the holograms operate as a uniaxial medium (the form-birefringence regime). In fact, the liquid crystal is a uniaxial medium that has to be optically compensated with similar optical media. From the results obtained in this study with holograms recorded at a wavelength of 413 nm, it is clear that the hologram moves away from the theoretical uniaxial behavior for illumination wavelengths in the blue region of the visible spectrum. To obtain a perfect form-birefringence regime over the whole visible spectrum, it would be necessary to use a smaller recording wavelength, for example, 363 nm (Argon laser), which is still compatible with photopolymer sensitivity.

The authors acknowledge fruitful discussions with B. Loiseaux, J. P. Huignard, and J. C. Lehureau of THALES Research and Technology FRANCE, Orsay, France. They are also grateful to the European Union for partial support of this work (OCDIS project).

## References

1. P. Yeh, *Optical Waves in Layered Media* (Wiley, New York, 1998).
2. A. Yariv and P. Yeh, *Optical Waves in Crystals* (Wiley, New York, 1994).
3. M. Born and E. Wolf, *Principles of Optics*, 6th ed. (Pergamon, New York, 1986).

4. J. P. Eblen, W. J. Gunning, D. Taber, P. Yeh, M. Khoshnevisan, J. Beedy, and L. Hale, "Thin-film birefringent devices based on form birefringence," in *Optical Thin Films IV: New developments," J. D. Rancourt, ed., Proc. SPIE* **2262,** 234–245 (1994).
5. G. Campbell and R. Kostuk, "Effective medium theory of sinusoidally modulated volume holograms," J. Opt. Soc. Am. A **12,** 1113–1117 (1995).
6. T. J. Kim, G. Campbell, and R. K. Kostuk, "Volume holographic phase retardation elements," Opt. Lett. **20,** 2030–2032 (1995).
7. C. Yang and P. Yeh, "Form birefringence of volume gratings in photopolymers," Appl. Phys. Lett. **69,** 3468–3470 (1996).
8. C. Yang and P. Yeh, "Artificial uniaxial and biaxial dielectrics with the use of photoinduced gratings," J. Appl. Phys. **81,** 23–29 (1997).
9. C. Joubert, J. C. Lehureau, L. Lee, F. Delauzun, and B. Morbieu, "TN-LCD viewing angle compensation with holographic volume gratings," in *Liquid Crystal Materials, Devices, and Applications VII*, R. Shashidhar, ed., Proc. SPIE **3635,** 137–142 (1999).
10. P. Lalanne and J. P. Hugonin, "High-order effective medium theory of subwavelength gratings in classical mounting: application to volume holograms," J. Opt. Soc. Am. A **15,** 1843–1851 (1998).
11. M. G. Moharam and T. K. Gaylord, "Three-dimensional vector coupled wave analysis of planar-grating diffraction," J. Opt. Soc. Am. **73,** 1105–1112 (1983).
12. H. Kogelnik, "Coupled wave theory for thick hologram grating," Bell Syst. Tech. J. **48,** 2909–2947 (1969).
13. M. Born and E. Wolf, *Principles of Optics*, 6th ed. (Pergamon, New York, 1986), pp. 694–699.
14. A. M. Weber, W. K. Smothers, T. J. Trout, D. J. Mickish, in *Practical Holography IV*, S. A. Benton, ed., Proc. SPIE **1212,** 30–39 (1990).
15. M. Born and E. Wolf, *Principles of Optics*, 6th ed. (Pergamon, New York, 1986), pp. 692–694.